MHD Simulation of Solar Chromospheric Evaporation Jets in the Oblique Coronal Magnetic Field

Y. Matsui, T. Yokoyama, H. Hotta and T. Saito

Department of Earth and Planetary Science, University of Tokyo, 7-3-1 Hongo, Bunkyo-ku, Tokyo 113-0033, Japan

ABSTRACT

We studied the MHD simulations of the chromospheric evaporation jet. The motivation of this work is to reproduce the characteristics of our observation result in the MHD simulation. In our simulations, two types of jets occur simultaneously caused by the magnetic reconnection between the oblique coronal magnetic field and emerged flux. The two types of the jets have the characteristics of the reconnection jet and evaporation jet respectively and consistent with the magnetic reconnection model. The reconnection jet and evaporation jet occur continuously. Continuous occurrence of the reconnection and evaporation jet is consistent with the interpretation of our observed jet.

Subject headings: Sun: corona — Sun: flares — Sun: magnetic fields

1. Introduction

Shibata et al. (1994) explained the jet as accelerated and heated by the magnetic reconnection between the emerging flux and coronal magnetic field. Two-dimensional MHD simulations performed by Yokoyama & Shibata (1995, 1996) successfully reproduced the characteristics of the jet based on this scenario. In their simulations, they did not succeed in reproducing the density of the observed jet. This is because a thermal conduction effect is not included in their simulations and then a chromospheric evaporation dose not occur. The chromospheric evaporation, i.e. acceleration by the high pressure caused through the thermal energy input from the magnetic reconnection site, may play a role to supply the density enhancement in the jet. The one-dimensional hydrodynamic simulations of the chromospheric evaporation were performed by Shimojo et al. (2001) and succeeded in reproducing the high density of the jet. Miyagoshi & Yokoyama (2004) extended the simulations of Yokoyama & Shibata (1995, 1996) and succeed in reproducing the evaporation flow by including the thermal conduction effect. They could reproduce the chromospheric evaporation in only

horizontal coronal magnetic field case. To understand the detail of the acceleration of the jet, however, the simulation of the chromospheric evaporation jet in the oblique coronal magnetic field is needed because the magnetic Lorenz force effects the acceleration of the jet and changes depending on the angle of the magnetic field. Furthermore, most of the jets are observed obliquely like our observed jet. By reproducing our observational results in the simulation, we can confirm our results.

Here we have succeeded in reproducing the chromospheric evaporation jet in the case of oblique coronal magnetic field. We also compare our simulation results with our observation.

2. Models

2.1. Magnetic Reconnection Model

The outline of our results is summarized in figures 1. In figures 1 (a) and (b), solid lines indicate the magnetic field. Figure 1 (a) shows the initial state of our simulation before the flux emergence occurs. There are an oblique magnetic field in the corona and flux sheet in the convection zone. After the addition of the perturbation in the flux sheet, the flux sheet is emerged by Parker instability (Parker 1966). The magnetic reconnection occurs between the coronal magnetic field and the emerged flux (figure 1 (b)). Since we assume an anomalous receptivity here, fast Petschek type (Petschek 1964) reconnection occurs (Yokoyama & Shibata 1994). After the reconnection, the heated and accelerated plasma is ejected as a reconnection jet. Simultaneously, the heat conduction occurs along the magnetic field to the chromosphere. The chromospheric plasma is accelerated by the high pressure and rises as an evaporation flow. Since this acceleration is caused by the thermal force, the evaporation flow is accelerated to around the sound speed. If the magnetic acceleration by the Lorenz force occurs, the evaporation flow is accelerated to beyond the sound speed.

2.2. Basic Equations

We assume nonlinear, time-dependent, resistive, compressible MHD fluids. A computation box is used with two-dimensional Cartesian coordinates with an uniform grid space in the $x-y$ plane. $\partial/\partial z = 0$, $V_z = 0$、 $B_z = 0$ are assumed. We solve MHD equations of the density ρ, pressure p, velocity $\boldsymbol{V}$ and magnetic field $\boldsymbol{B}$:

$$\frac{\partial \rho}{\partial t} + \boldsymbol{\nabla} \cdot (\rho \boldsymbol{V}) = 0, \tag{1}$$

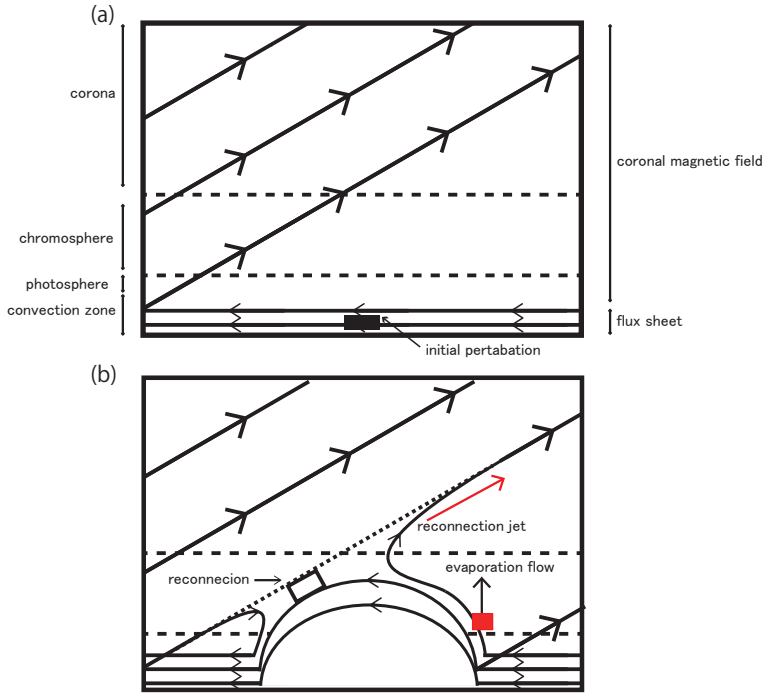

Fig. 1.— The outline of our results. Solid lines indicate the magnetic field. (a) shows the initial state before the flux emergence occurs and (b) shows the magnetic reconnection between the coronal magnetic field and the emerged flux.

$$\frac{\partial}{\partial t}(\rho \boldsymbol{V}) + \boldsymbol{\nabla} \cdot \left[\rho \boldsymbol{V}\boldsymbol{V} + \left(p + \frac{\boldsymbol{B}^2}{8\pi} \right) \xi - \frac{\boldsymbol{B}\boldsymbol{B}}{4\pi} \right] = \rho \boldsymbol{g}, \tag{2}$$

$$\frac{\partial}{\partial t}(\boldsymbol{B}) + c\nabla \times \boldsymbol{E} = 0, \tag{3}$$

$$\begin{aligned} \frac{\partial}{\partial t}\left(\frac{p}{\gamma - 1} + \frac{1}{2}\rho V^2 + \frac{B^2}{8\pi} \right) &+ \nabla \cdot \left((\frac{\gamma}{\gamma - 1} p + \frac{1}{2}\rho V^2)\boldsymbol{V} + c\frac{\boldsymbol{E} \times \boldsymbol{B}}{4\pi} \right) \\ &- \rho \boldsymbol{g} \cdot \boldsymbol{V} = \nabla \cdot (\kappa_{\parallel} \nabla_{\parallel} T) - R + H, \end{aligned} \tag{4}$$

$$\boldsymbol{E} = \frac{4\pi}{c^2}\eta \boldsymbol{J} - \frac{1}{c}\boldsymbol{V} \times \boldsymbol{B}, \tag{5}$$

$$\boldsymbol{J} = \frac{c}{4\pi}\boldsymbol{\nabla} \times \boldsymbol{B}, \tag{6}$$

$$p = \frac{k_{\mathrm{B}}}{m}\rho T. \tag{7}$$

Here $\gamma = 5/3$, ξ, k_B, $m = (1/2)m_p$, c, $\boldsymbol{g}$, R and H are specific heat ratio, the unit tensor, Boltzmann constant, mean molecular mass, light speed, gravitational acceleration, radiative cooling and coronal heating, respectively. The gravitational acceleration is constant and parallel to the y-direction. We assume a Spitzer-type anisotopic heat conduction working only in the direction of the magnetic field. $\kappa_{\parallel}$ is a conductivity along the magnetic field and $\kappa_{\parallel} = \kappa_0 T^{5/2}$. κ_0 is 1×10^{-6} in the cgs units. The radiative cooling is described by the formula:

$$R = \rho^2 \cdot \Lambda_\rho(\rho) \cdot \Lambda(T) \tag{8}$$

$$\Lambda_\rho(\rho) = (\rho_{cl}/\rho)\tanh(\rho/\rho_{cl}) \tag{9}$$

The dependence on the density $\Lambda_\rho(\rho)$ is due to the optical depth in assumption with its change to optically thick regime at $\rho = \rho_{\rm cl} = 10^{12}{\rm cm}^{-3}$. $\Lambda(T)$ is a radiative loss function of an optically thin plasma and is estimated by the formula:

$$\Lambda(T) = \chi T^{\alpha} \tag{10}$$

where $\chi(T)$ and $\alpha(T)$ is summarized in table 1. The radiative loss below $4\times10^4 K$ is neglected. The coronal heating is assumed to be working above the transient region in a steady manner

T(K)	α	χ	Reference
$4 \times 10^4 < T < 1 \times 10^5$	3.0	8.00×10^{-37}	1
$1 \times 10^5 < T < 3 \times 10^5$	0.0	8.00×10^{-22}	1
$3 \times 10^5 < T < 8 \times 10^5$	-2.5	3.94×10^{-8}	2
$8 \times 10^5 < T < 2 \times 10^7$	-1.0	5.51×10^{-17}	2
$2 \times 10^7 < T$	0.4	3.31×10^{-27}	3

Table 1: References. -(1)Sterling et al. (1993);(2)Hildner (1974); Nagai (1980).

and is given as $H = 5.0 \times 10^{-4}$ergs cm^{-3} s^{-1}. This coronal heating and radiation is the same type in Hori et al. (1997).

We assume the anomalous resistivity:

$$\eta = \begin{cases} \eta_{\rm st} & \text{for } v_d < v_c, \\ \eta_{\rm st} + \eta_{\rm an}\left(v_d/v_c - 1\right)^2 & \text{for } v_c \le v_d \le v_{\rm dmax}, \\ \eta_{\rm max} & \text{for } v_d \ge v_{\rm dmax}, \end{cases} \tag{11}$$

where $v_{\rm dmax}$ is the value of v_d when $\eta = \eta_{\rm max}$.

The units of length, velocity and time is $\mathcal{H}_0$、 $C_{\rm S0}$, $\tau_0 \equiv \mathcal{H}_0/C_{\rm S0}$, respectively. $\mathcal{H}_0$ and $C_{\rm S0}$ are pressure scale height $\mathcal{H} \equiv p/(\rho g)$ at the photosphere ($y = 0$) and sound speed $C_{\rm S} \equiv \sqrt{\gamma p/\rho}$, respectively. Density is normalized by the ρ_0 at the photosphere ($y = 0$).

2.3. Initial Condition

The picture of initial condition of our simulation is described in figure 1 (a). A computation region is $0 < x < 80, -3 < y < 80$. The number of grid points is $[x, y] = [512, 1024]$. We assume a periodic condition at $x = 0$ and 80 and a symmetric condition at $y = -3$ and 80.

The initial magnetic field is assumed as

$$B_x(y) = [8\pi p(y)\alpha(y)]^{1/2} + B_{\rm add}\cos\theta, \tag{12}$$

$$B_y(x) = B_{\rm add}\sin\theta., \tag{13}$$

$$\alpha(y) = \alpha_f f(y), \tag{14}$$

$$f(y) = \frac{1}{4}\left[\tanh\left(\frac{y-y_0}{w_f}\right)+1\right]\left[-\tanh\left(\frac{y-y_1}{w_f}\right)+1\right]. \tag{15}$$

The initial distribution of the emerging flux is given by α_f. The coronal magnetic field is given by $B_{\rm add}$. We take $\alpha_f = 0.1, w_f = 0.5, y_0 = -2.0, y_1 = 0.0$. θ is the angle between the coronal magnetic field and x-axis. In our simulation, we take $\theta = \pi/6$ which is similar to our observation.

In the initial condition, we take the coronal temperature $T_{\rm cor}$ as 100 times hotter than photospeheric temperature $T_{\rm pho}$. The initial distribution of the temperature above $y = 0$ is given by

$$T(y) = T_{\rm pho} + (T_{\rm cor} - T_{\rm pho}) \times \left\{\frac{1}{2}\left[\tanh\left(\frac{y-y_{\rm tr}}{w_{\rm tr}}\right)+1\right]\right\} \quad \text{for } y \geq 0, \tag{16}$$

where $y_{\rm tr}$ and $w_{\rm tr}$ are the height and the width of the transient region respectively. We take $y_{\rm tr} = 8.0$ and $w_{\rm tr} = 0.5$. The temperature distribution of the photosphere is given by

$$T(y) = T_{\rm pho} - \left(a\left|\frac{dT}{dy}\right|_{\rm ad}\right) y \quad \text{for } -3 \leq y \leq 0, \tag{17}$$

where $|dT/dt|_{\rm ad} \equiv (\gamma - 1)/\gamma$ is the adiabatic temperature gradient and a is the dimensionless constant of order unity. When $a > 1$, this layer becomes unstable for the convective instability and we take $a = 2$. The initial density distribution is a stratification under the uniform gravity. Note that our initial condition is dynamically in equilibrium but thermally in non-equilibrium because of the existence of the heat conduction effect.

We use CIP method for the MHD part and SOR method for the anisotopic heat conduction part in our simulation. All code are included in CANS (Coordinated Astronomical

Numerical Software) code maintained by Yokoyama et al. [1]

3. Results

Figures 2-3 are results of our simulation. The color contours of the top panels of figures 2-3 show the density. Solid lines and vectors in the top panels indicate the magnetic field and velocity respectively. The bottom panels show the one-dimensional distributions of the density, velocity, temperature and pressure along the magnetic field indicated by the white lines on the top panels. The white lines in figures 2-3 correspond to the same magnetic field. The horizontal axis of the bottom panels show the height.

Because of the perturbation in the flux sheet, the flux emergence occurs in figure 2. The magnetic reconnection occurs between the coronal magnetic field and emerged flux. The magnetic reconnection occurs around the time $t = 88.5$, on the traced magnetic field indicated by the white lines. The magnetic field indicated by the white line is strongly bended. The strongly bended magnetic field becomes straight $t = 89.2$. The high velocity jet occurs around the reconnection point, $y = 20$, and the velocity is around the Alfvén velocity of the inflow region. The acceleration mechanism of this jet is consistent with that of the reconnection jet, i.e. the acceleration by the magnetic force. Because of the magnetic reconnection, the steep gradient of the temperature is formed and proceeds toward the chromosphere during the period shown. Then the temperature and pressure of the upper chromosphere rise and the highly dense jet occurs from the upper chromosphere in figure 3. The density of this jet is 5 times denser than background corona. The velocity of this jet is around the sound speed of the heated chromospheric plasma. The acceleration mechanism of this jet is consistent with that of the chromospheric evaporation jet, i.e. the acceleration by the thermal force.

4. Discussion

From the one-dimensional plots in figures 2 - 3, it seems that a reconnection jet and an evaporation jet are reproduced simultaneously. This implies that the magnetic and thermal acceleration occur simultaneously. This multi acceleration in the jet is consistent with the result of our observations. In our simulations, the reconnection jet occurs first and then the

---

[1]CANS (Coordinated Astronomical Numerical Software) is available online at: `http://www-space.eps.s.u-tokyo.ac.jp/~yokoyama/etc/cans/`

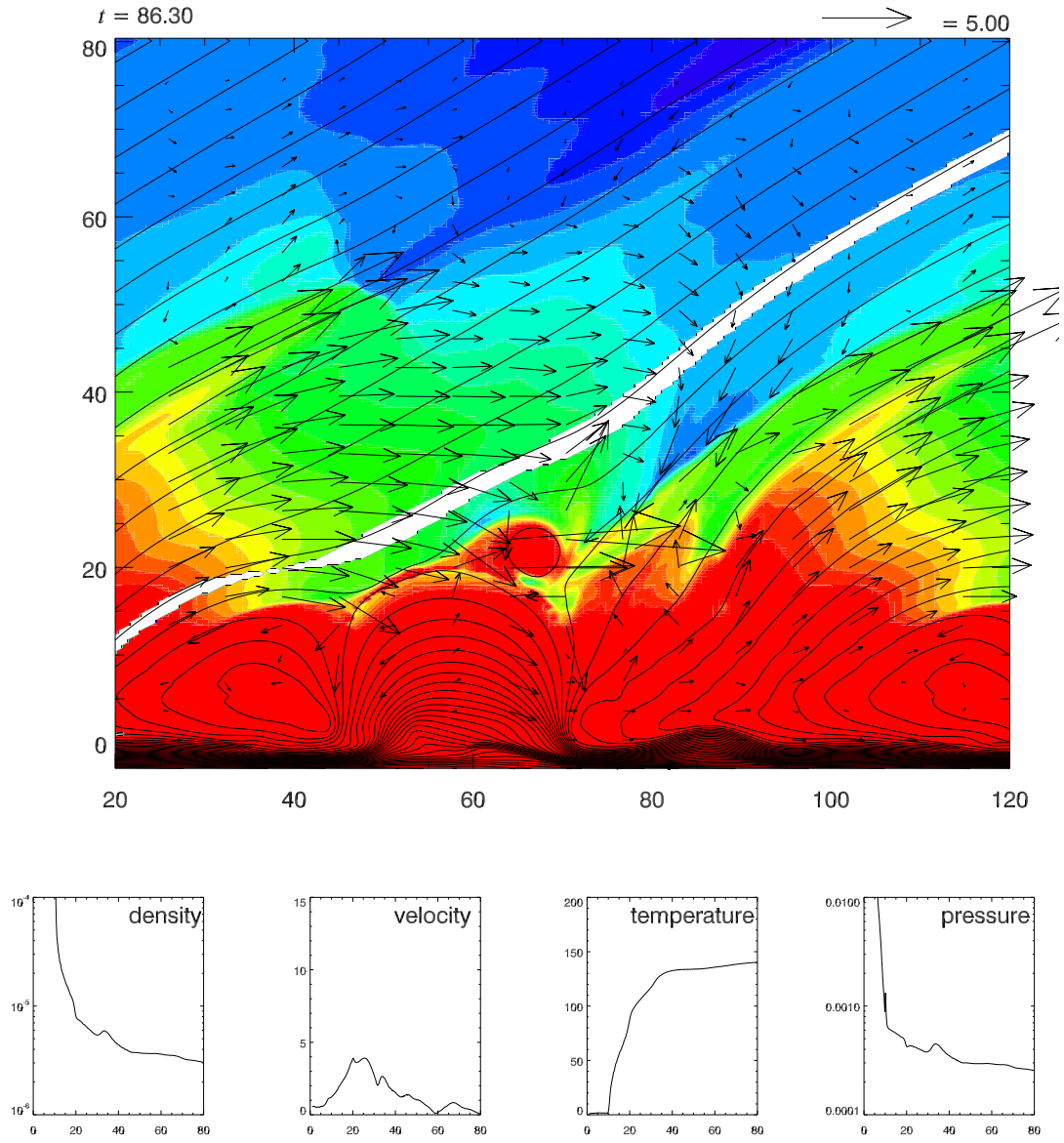

Fig. 2.— The results of our simulation at $t = 86.3$. The color contours of the top panel show the density and solid lines and vectors indicate the magnetic field and velocity respectively. The bottom panels show the one-dimensional distribution of the density, velocity, temperature and pressure along the magnetic field indicated by the white lines on the top panel. The horizontal axis of the bottom panels show the height.

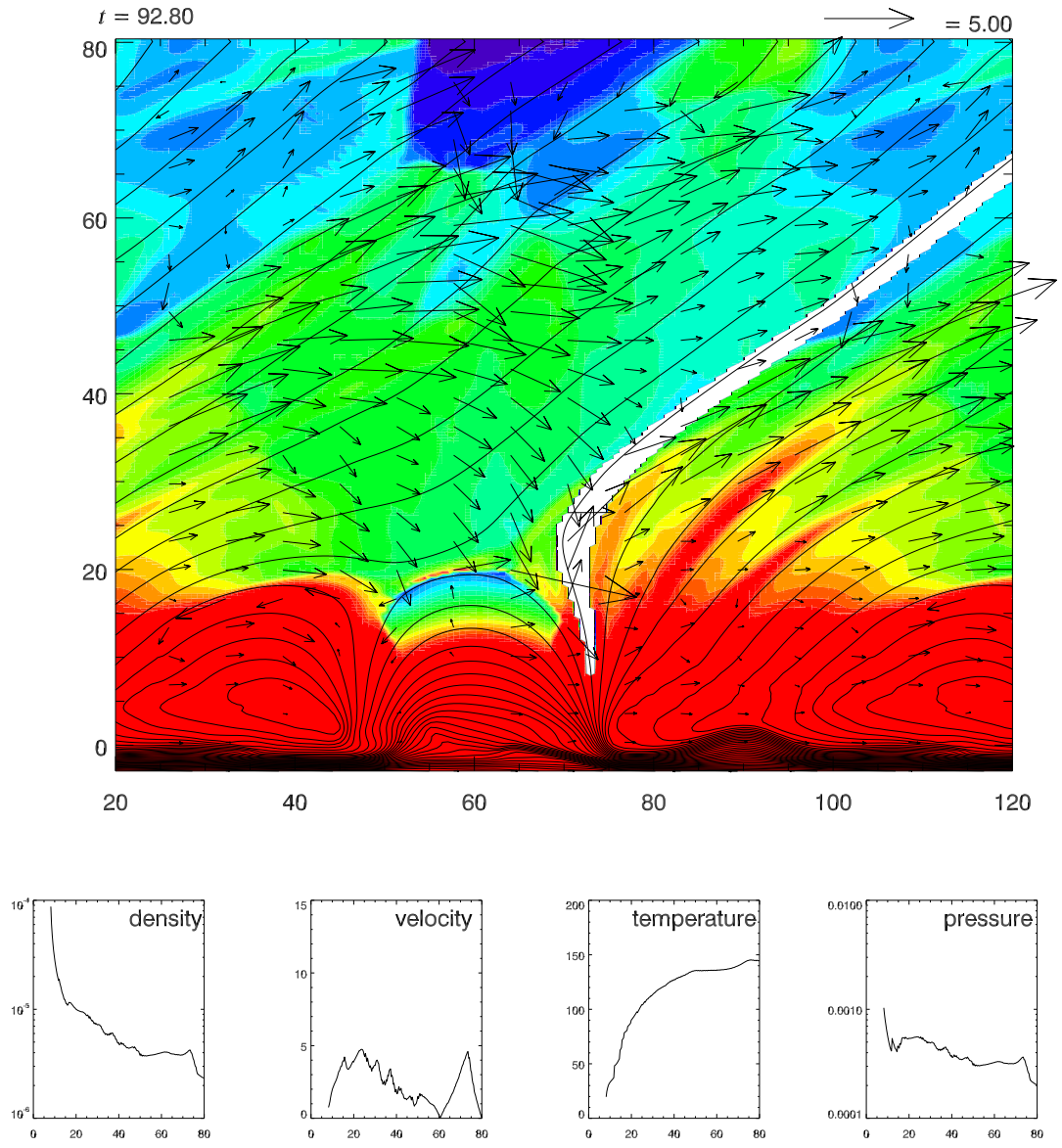

Fig. 3.— Same figures as figure 2 at $t = 88.5$. The white line corresponds to the line on the top panel of figure 2.

evaporation occurs secondly. The time rag between the reconnection jet and evaporation jet is almost same as the thermal conduction time and is around 1 min in the real scale. The reconnection jet and evaporation jet are mixed after the evaporation jet occurs. This is because the magnetic field is weak in our simulation and the velocity of the reconnection jet is almost same as that of the evaporation jet. In more strong magnetic field case like the real corona, Alfvén velocity is much faster than the sound speed. In such case, the reconnection jet and evaporation jet would not be mixed after the evaporation jet occurs.

5. Summary

We have reproduced the reconnection and evaporation jet simultaneously in the oblique coronal magnetic field. In our simulations, two types of the jets occur caused by the magnetic reconnection between the oblique coronal magnetic field and emerged flux. The two types of the jets have the characteristics of the reconnection jet and evaporation jet respectively and consistent with the magnetic reconnection model. The reconnection jet and evaporation jet occur simultaneously. Simultaneous occurrence of the reconnection and evaporation jet is consistent with the interpretation of our observed jet.

REFERENCES

Hildner, E. 1974, Sol. Phys., 35, 123

Hori, K., Yokoyama, T., Kosugi, T., & Shibata, K. 1997, ApJ, 489, 426

Miyagoshi, T., & Yokoyama, T. 2004, ApJ, 614, 1042

Nagai, F. 1980, Sol. Phys., 68, 351

Parker, E. N. 1966, ApJ, 145, 811

Petschek, H. E. 1964, NASA Special Publication, 50, 425

Shibata, K., Nitta, N., Matsumoto, R., Tajima, T., Yokoyama, T., Hirayama, T., & Hudson, H. 1994, in X-ray solar physics from Yohkoh, ed. Y. Uchida, T. Watanabe, K. Shibata, & H. S. Hudson, 29–+

Shimojo, M., Shibata, K., Yokoyama, T., & Hori, K. 2001, ApJ, 550, 1051

Sterling, A. C., Shibata, K., & Mariska, J. T. 1993, ApJ, 407, 778

Yokoyama, T., & Shibata, K. 1994, ApJl, 436, L197

—. 1995, Nature, 375, 42

—. 1996, PASJ, 48, 353